

A number of new derivatives of pyrimido[4,5-*c*]pyridazine have been synthesized from the treatment of 6-acetyl-3-amino-2,5-diphenyl-2,5-dihydropyridazine-4-carbonitrile (**1**) as precursor with various reactants obtained quantitatively the desired products (**2**), (**5**), (**7**), and (**9a–e**). The structures of all the synthesized products have been elucidated thoroughly. The potential AKT1 inhibitory activities of these new synthesized compounds have also been studied by docking calculations, which have been performed in Gold 5.2 software using Genetic algorithm.

J. Heterocyclic Chem., **00**, 00 (2015).

INTRODUCTION

A large number of biologically active compounds containing pyrimido[4,5-*c*]pyridazine structure have been described. These compounds are useful in human therapy because of their inhibitory activities of AKT [1], monoamine oxidase [2], phosphodiesterase 5 (PDE5) [3,4], selective human A1 adenosine receptor ligands [5], and p38R [6].

Several synthetic routes for the construction of pyrimidopyridazines have been found in the literature. 3-Aminopyridazine was condensed with 1,3-dicarbonyl compounds in polyphosphoric acid to give the related pyrimidopyridazine [7]. The reaction between bromoacetone and 6-hydrazinoisocytosine were afforded pyrimidopyridazine in low yield [8]. 6-(1-Alkylhydrazino)isocytosines have been also reported to cyclize with 1,3-diketo esters or with simple α -keto esters to give the corresponding pyrimido[4,5-*c*]pyridazines in good yields [9,10]. Morrison and co-workers were described the cyclizations of glyoxals with 6-hydrazinoisocytosines [11] while the synthesis of 3-(substituted)pyrimido[4,5-*c*]pyridazine-5,7(1*H*,6*H*)-diones were performed by Turbiak through the condensation of 3-methyl-6-(1-methylhydrazinyl)uracil with phenyl and alkyl glyoxal monohydrates [12]. A series of new 4-aryl-6,8-dimethylpyrimido[4,5-*c*]pyridazine-5,7(6*H*,8*H*)-dione derivatives were synthesized via three component reactions of 1,3-dimethylbarbituric acid with arylglyoxals in the presence of hydrazinium dihydrochloride [13,14].

On the other hand, AKT1 is a member of the serine/threonine AGC protein kinase family. It is frequently overexpressed and active in many types of human cancers including cancers of colon, breast, brain, pancreas and prostate as well as lymphomas and leukemias. Some clinical trials are in progress to test the efficacy of AKT pathway inhibitors in treating cancer. Inhibitor VIII as the most reported effective compound for the inhibitory of AKT1 and the crystal structure of AKT1 complexed to inhibitor VIII (PDB:3O96) have been reported in the literature [15].

Hence, these observations prompted us to synthesize new derivatives of pyrimido[4,5-*c*]pyridazine and evaluating of them as potential AKT1 inhibitors.

RESULTS AND DISCUSSION

Chemistry. According to the reported procedure [16–18], the preparation of precursor (**1**) is started from the reaction of benzenediazonium salt with ethyl 3-oxobutanoate to give 1-(2-phenylhydrazono)propan-2-one. On the other hand, 2-benzylidenemalonitrile is obtained from the treatment of benzaldehyde and malononitrile. Consequently, the reaction of the latter compound with 1-(2-phenylhydrazono)propan-2-one in EtOH gives the precursor (**1**) quantitatively.

The capability of the precursor (**1**) in the synthesis of new derivatives of pyrimido[4,5-*c*]pyridazines heterocyclic ring system was initially carried out by treatment of

Table 1

Experimental and theoretical chemical shift values of the compounds shown in Figure 2, calculated at mPW1PW91/6-31G(d)-PCM.^a

Entry	C5	$ \Delta\delta ^b$	C6	$ \Delta\delta ^c$
8	179.35	0.33	165.47	11.14
8*	152.49	27.19	168.24	8.37
Exp.	179.68	—	176.61	—
9a	168.31	1.01	167.92	1.33
9a*	142.74	26.58	172.01	2.76
Exp.	169.32	—	169.25	—
9b	168.35	0.88	167.61	1.22
9b*	142.75	26.48	172.01	3.18
Exp.	169.23	—	168.83	—
9c	168.38	0.88	167.59	1.28
9c*	142.62	26.64	172.02	3.15
Exp.	169.26	—	168.87	—
9d	168.42	0.87	167.58	1.34
9d*	142.6	26.69	172.03	3.11
Exp.	169.29	—	168.92	—
9e	168.07	0.66	167.34	0.95
9e*	145.85	22.88	172.04	3.75
Exp.	168.73	—	168.29	—

^aAcetone-d₆ for compounds **8** and **8*** and CDCl₃ for other compounds.

^b $|\Delta\delta|$ = absolute deviation chemical shift for C5 from experimental data.

^c $|\Delta\delta|$ = absolute deviation chemical shift for C6 from experimental data.

compound (**1**) with phenyl isocyanate in the mixture of KOH in dry dimethylformamide at room temperature to afford compound (**2**) (Scheme 1).

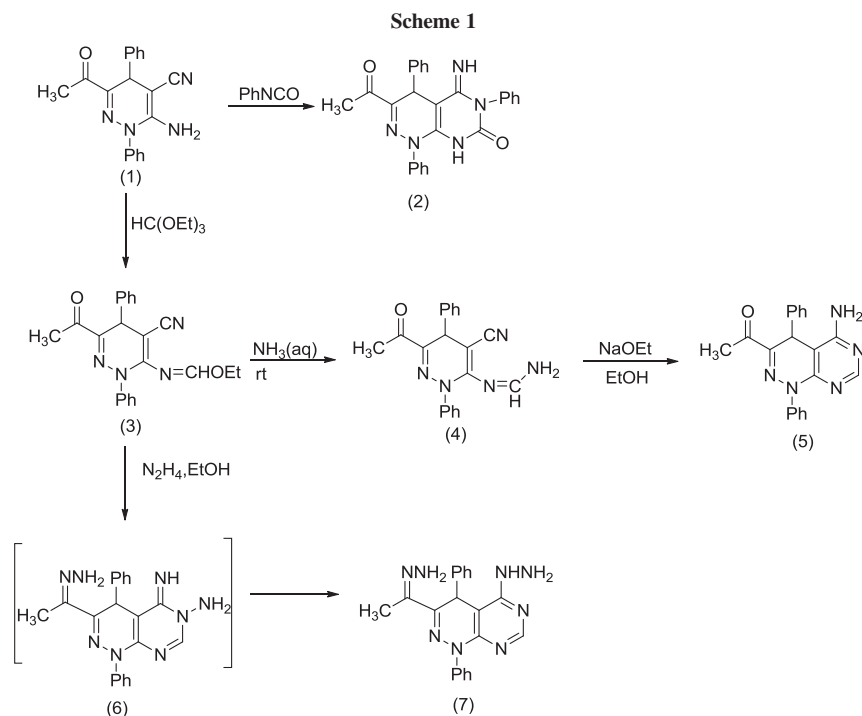
The ¹H-NMR spectrum of compound (**2**) shows a singlet signal at δ 2.40 ppm indicating the presence of CH₃ group, a broad singlet signal at δ 5.05 ppm due to NH group,

which was removed on deuteration, a singlet signal at δ 5.25 ppm due to CH group in the pyridazine ring, a broad singlet signal at δ 7.10 ppm due to C=NH group, a multiplet signal at δ 7.20–7.70, which are corresponded to the hydrogens of phenyl moieties. In IR spectrum, the disappearing of stretching vibration band of CN group at 2194 cm⁻¹ and NH₂ at 3412 and 3309 cm⁻¹ and appearing of a sharp peak due to NH group at 3125 cm⁻¹ also confirm the new ring closure.

Moreover, precursor (**1**) is refluxed in a mixture of triethylorthoformate and anhydride acetic acid to give compound (**3**). Then, the stirring of a mixture of (**3**) and 25% NH₃(aq) in ethanol at room temperature affords (**4**). The treatment of (**4**) with NaOEt in EtOH obtains quantitatively product (**5**) as another new synthesized heterocyclic compound of pyrimido[4,5-*c*]pyridazine (Scheme 1).

The ¹H-NMR spectrum of compound (**5**) shows a singlet signal at δ 2.33 ppm indicating the presence of CH₃ group, a singlet signal at δ 5.55 ppm due to CH group in the pyridazine ring, a broad signal at δ 7.05 ppm due to NH₂ group, a multiplet signal at δ 7.21–7.70, which are corresponding to hydrogens of aromatic rings, and a singlet signal at δ 8.05 ppm due to the hydrogen of the new fused pyrimidine ring.

On the other hand, a mixture of compound (**3**) and hydrazine hydrate is refluxed in dry ethanol to give first the intermediate (**6**), which is isomerized to thermodynamically stable product (**7**) through Dimroth rearrangement (Scheme 1). In the protocol led to the formation of compound (**7**), a nucleophilic condensation reaction on



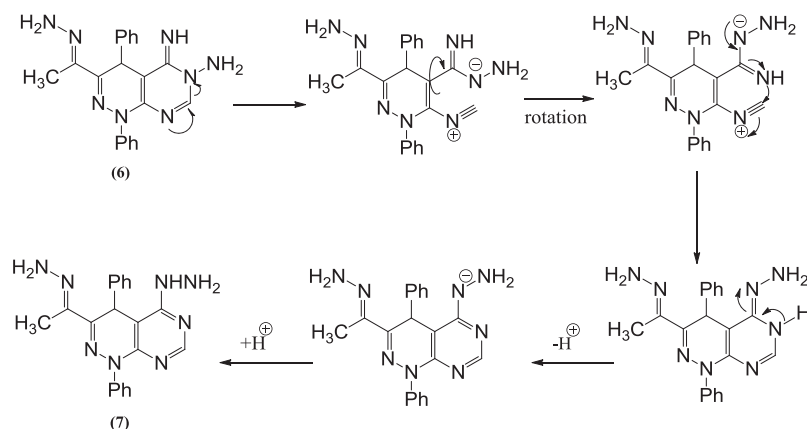
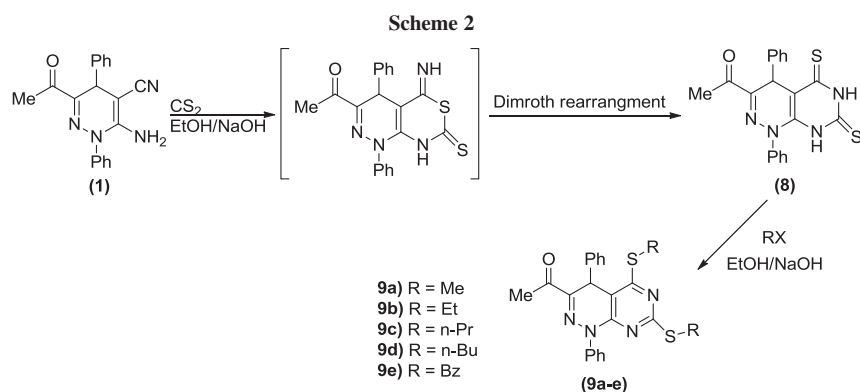


Figure 1. The chemical mechanism of the preparation of compound (7) via Dimroth rearrangement.



the carbonyl group of compound (6) is taken place by hydrazine. The spectral and microanalytical data of the synthesized compound (7), summarized in the experimental section, confirm the desired structure.

The plausible mechanism of this rearrangement could be explained as depicted in Figure 1. The similar results about this rearrangement are in agreement with the reported results for analogous compounds [19].

On the other hand, the reaction of precursor (1) with CS_2 was carried out to obtain the related cyclized product, which is consequently further alkylated with various alkylhalides (Scheme 2).

According to the literature review, there are at least two different published methods about the treatment with CS_2 , which give the corresponding heterocyclized product [20,21]. As a good criterion, the density functional theory calculations can be applied to evaluate the structures of the products (8) and (9a-e) [22]. Hence, the mPW1PW91 method and 6-31G(d) basis set were utilized to calculate the optimized structures (Fig. 2). The energy difference between the proposed regioisomers (8) and (9a-e) and the corresponding ones, (8)* and (9a-e)*, are listed in Table 1. The calculated results show that compounds (8) and (9a-e) are more stable than the other regioisomers.

Furthermore, the chemical shifts of C5 and C6 identified in Figure 2 are crucial in deducing of the real structures; therefore, the ^{13}C -NMR chemical shifts were also computed and applied as another criterion. The calculated ^{13}C -NMR chemical shifts of (8) and (9a-e) compared with the corresponding ones of (8)* and (9a-e)* are qualitatively in close agreement with the experimental data (Table 1). Eventually, the depicted structures of compounds (8) and (9a-e) in Scheme 2 are the true structures, which are obtained through the reaction conditions.

The spectral and microanalytical data of all the newly synthesized compounds (8) and (9a-e) are fully characterized. The 1H -NMR spectrum of compound (8) shows a

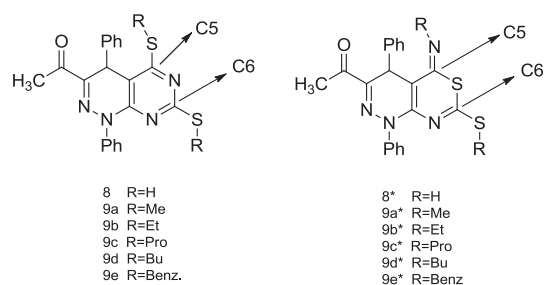


Figure 2. The proposed structures for the computational calculations.

singlet signal at δ 2.38 ppm indicating the presence of CH_3 group, a singlet signal at δ 5.89 ppm due to CH signal of pyridazine ring, a multiplet peak at δ 7.21–7.70 ppm belonging to hydrogen signals of phenyl groups, two broad singlet signals at δ 7.14 and 10.24 ppm corresponding to two protons indicating the presence of two NH groups, which are disappeared by adding D_2O . In the IR spectrum, the disappearance of stretching vibration band of CN group of the precursor (**1**) at 2194 cm^{-1} and NH_2 at 3412 and 3309 cm^{-1} and disclosing of a peak at 3125 cm^{-1} for NH group also confirm the occurrence of the desired heterocyclization.

On the other hand, the $^1\text{H-NMR}$ spectrum of compound (**9a**), as an example, shows three singlet signals at δ 2.36, 2.44, and 2.52 ppm corresponding to three CH_3 groups, a singlet signal at δ 5.47 ppm due to CH group in the pyridazine ring, a multiplet signal at δ 7.22–7.67, which is corresponded to ten hydrogens of aromatic rings. The disappearance of two broad singlet signals of NH groups of compound (**8**) is another reason to confirm the alkylation of compound (**8**). The disappearance of vibration band of NH group in the IR spectrum of compound (**9a**) as well as the occurrence of molecular ion peak at m/z 420 clearly confirms the synthesis of compound (**9a**).

The plausible mechanism for compound (**8**) can be explained by Dimroth rearrangement, which is an isomerization that consists in a translocation of sulfur and nitrogen through a ring-opening-ring-closure sequence as depicted in Figure 3 [23].

Molecular docking. Docking is carried out using Genetic Optimization for Ligand Docking (Gold) software based on Goldscore fitness function that uses the Genetic algorithm (GA). All water molecules and hetero atoms are removed from the protein to evaluate the scoring function in Goldsoftware. For each of the 50 independent GA runs, a maximum number of 100 000 GA operations are performed on a set with a population size of 100 individuals. Operator weights are set to 95, 95, and 10 for crossover, mutation, and migration, respectively. Default cutoff values of 2.5 \AA (dH-X) for hydrogen bonds and 4.0 \AA for Van der Waals distance are employed. The root mean square deviation values for the docking calculations are based on the root mean square deviation matrix of the ranked solutions. We observed that the best ranked solutions are always among the first 50 GA runs, and the conformation of the molecules based on the best fitness score is further analyzed.

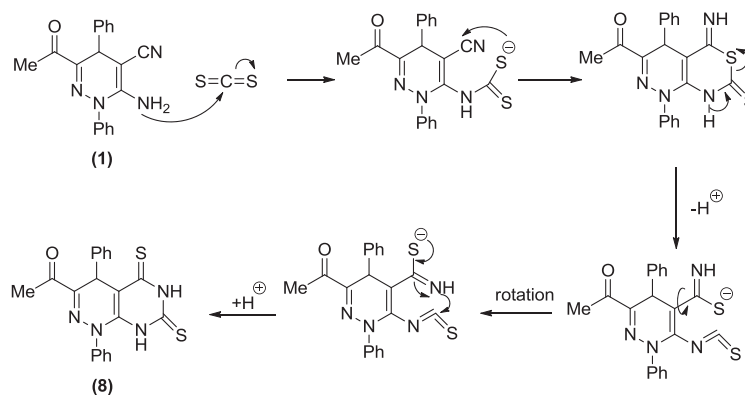


Figure 3. The chemical mechanism of the preparation of compound (**8**) via Dimroth rearrangement.

Table 2

The data obtained from docking studies of compounds (**2**), (**5**), (**7**), (**8**), and **9** (a–e), on inhibitory activities of AKT1.

Entry	Goldscore	ΔG_d (kJ/mol)	K_i	H-B	Pi-Pi	Pi- σ	VdW-B
2	68.37	-36.55	$3.94\text{e-}07$	2	3	—	—
5	67.96	-23.76	$6.86\text{e-}05$	2	2	—	1
7	65.98	-28.88	$8.71\text{e-}06$	5	1	—	1
8	81.19	-24.66	$4.77\text{e-}05$	3	2	—	2
9a	69.81	-34.61	$8.62\text{e-}07$	1	—	—	—
9b	75.32	-31.61	$2.90\text{e-}06$	3	3	—	1
9c	85.75	-41	$6.56\text{e-}08$	2	—	—	—
9d	76.51	-36.78	$3.60\text{e-}07$	1	1	—	1
9e	99.32	-49.5	$2.12\text{e-}09$	2	3	1	—
Co-Crystal	87.89	-35.96	$5.02\text{e-}07$	2	5	—	1

ΔG_d : final docked energy; K_i : estimated inhibitory constant; H-B, the number of hydrogen bond; Pi-Pi, the number of Pi-Pi interactions, Pi- σ : the number of Pi- σ interactions.

Because of the lots of reported articles on the importance of anticancer activities of pyridazine derived heterocyclic compounds and our interests on the assessment of inhibitory activities of AKT1, the docking of the newly synthesized compounds (**2**), (**5**), (**7**), (**8**), and (**9a-e**) with AKT1 (PDB ID: 3O96) are performed by using of Goldscore

fitness function. The algorithm exhaustively searches the entire rotational and translational space of the ligand with respect to the receptors. The various solutions evaluate by a score which is equivalent to the absolute value of the total energy of the ligand in the protein environment. The best docking solutions of Goldscore for each compound is

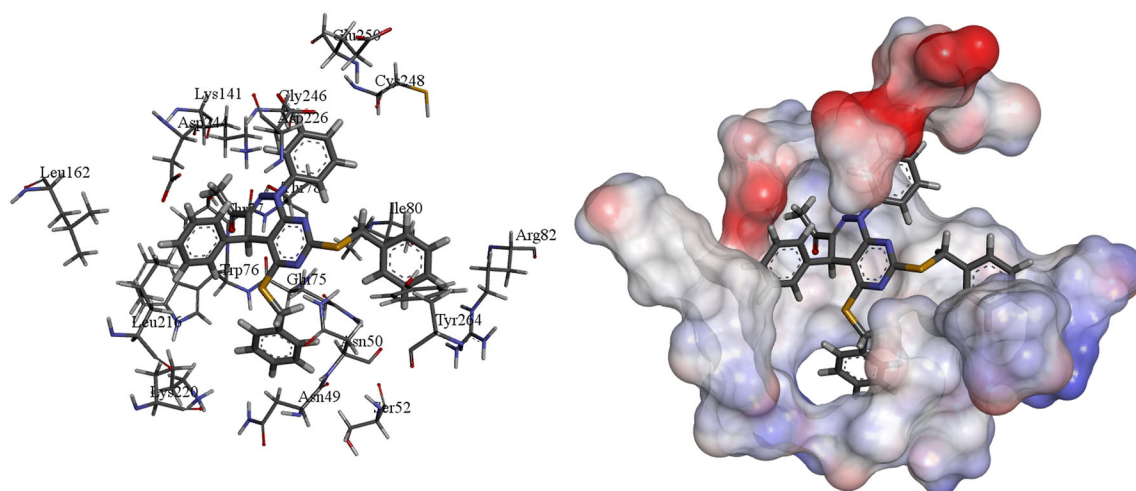


Figure 4. The best docked structure of (**9e**) in the active site pocket of AKT1 (PDB Code: 3O96, flexible residue: TRP80- ILE84- SER205- LYS268- TYR272- ILE290- ASP292- CYS296 in stick (left) and solvent surface (right) views. [Color figure can be viewed in the online issue, which is available at wileyonlinelibrary.com.]

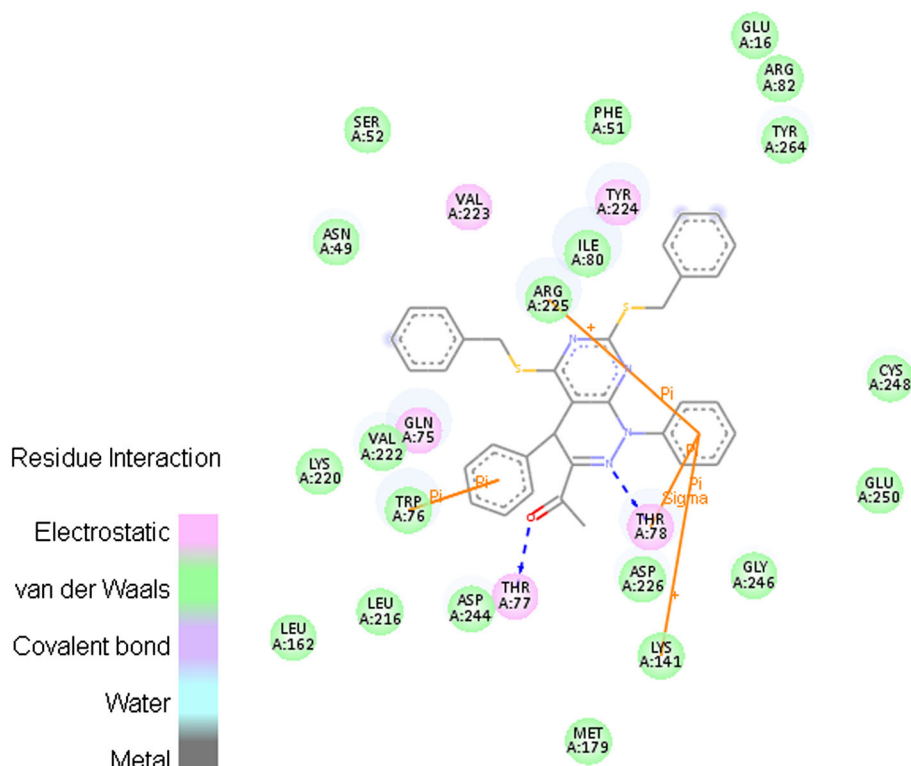


Figure 5. The 2D representation of the interaction between compound (**9e**) in the crystal structure of AKT1 (PDB Code: 3O96) using of Goldscore fitness function. Blue dashed line: hydrogen bond (THR A:78, THR A:77), brown line: $\text{P}_i\text{-P}_i$ interaction (TRP A:76, LYS A:141, ARG A:225), $\text{P}_i\text{-}\sigma$ interaction (THR A:78). [Color figure can be viewed in the online issue, which is available at wileyonlinelibrary.com.]

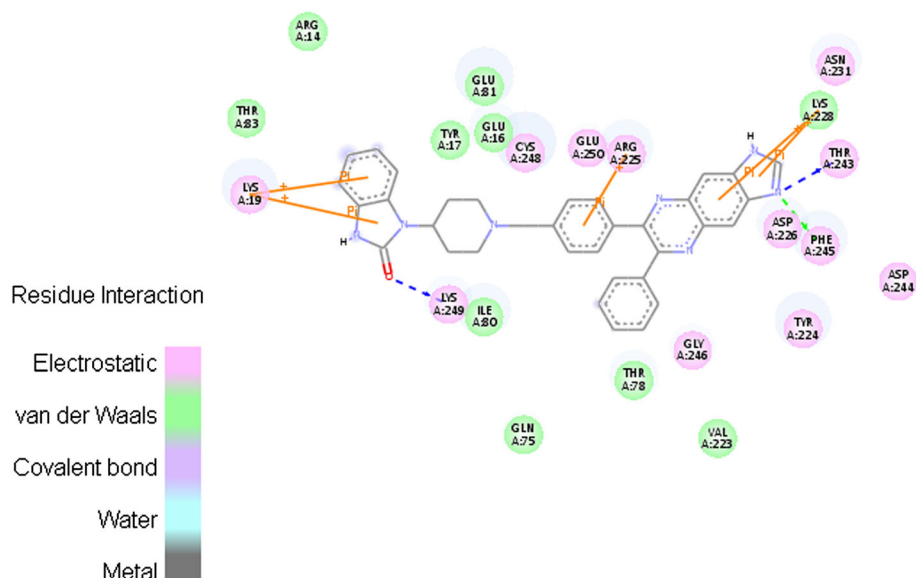


Figure 6. The 2D representation of the interaction between Co-Crystal in the crystal structure of AKT1 (PDB Code: 3O96) using of Goldscore fitness function. Blue dashed line: hydrogen bond (THR A: 243, LYS A: 249), green line: Van der Waals bond (PHE A: 245), brown line: P₁-P_i interaction (LYS A: 19, LYS A: 228, ARG A: 225). [Color figure can be viewed in the online issue, which is available at wileyonlinelibrary.com.]

considered. Goldscore performs a force field based on scoring function and is made up of four components:

- 1) Protein-ligand hydrogen bond energy (external H-bond).
- 2) Protein-ligand Van der Waals energy (external vdw).
- 3) Ligand internal Van der Waals energy (internal vdw).
- 4) Ligand interamolecular hydrogen bond energy (internal-H-bond).

The external vdw score is multiplied by a factor of 1.375 when the total fitness score is computed. This is an empirical correction to encourage protein-ligand hydrophobic contact. The fitness function has been optimized for the prediction of ligand binding positions. $\text{Goldscore} = S_{(\text{hb_ext})} + S_{(\text{vdw_ext})} + S_{(\text{hb_int})} + S_{(\text{vdw_int})}$, where $S_{(\text{hb_ext})}$ is the protein-ligand hydrogen bond score, $S_{(\text{vdw_ext})}$ is the protein-ligand Van der Waals score, $S_{(\text{hb_int})}$ is the score from interamolecular hydrogen bond in the ligand, and $S_{(\text{vdw_int})}$ is the score from intramolecular strain in the ligand. The possible active site is identified using Accelrys DS Visualizer. Eight active site residues as TRP80- ILE84- SER205- LYS268- TYR272- ILE290- ASP292- CYS296 are found by the removal of inhibitor VIII. Therefore, it is chosen as the most biologically favorable site for docking.

The estimated inhibitory constants of the mentioned docked compounds as well as Goldscore, free energy of binding, and the whole interactions among the moieties of the products are shown in Table 2.

The evaluation of the results in Table 2 and the comparison of Goldscores, ΔG_d , and K_i of the newly synthesized compounds with Co-Crystal demonstrate that compounds (2) and (9c–e) have the considerable results in comparison

with Co-crystal. The authors think the Pi-Sigma interaction in compound (9e), which shows the best results in Table 2, can be important on the potent inhibitory effect of AKT1 in comparison with the other synthesized compounds and even co-crystal (Figs. 4–6).

CONCLUSION

The chemical procedures outlined provided very simple and straightforward routes to obtain various derivatives of pyrimido[4,5-*c*]pyridazine. The designed and synthesized compounds were studied as potential AKT1 inhibitory activity, and the results showed that compound (9e) had better inhibitory effect than the other compounds and even co-crystal. Further studies are in progress to improve our knowledge of the SAR of this inhibitory activity.

EXPERIMENTAL

Melting points were recorded on an Electrothermal type 9100 melting point apparatus. The IR spectra were obtained on Avatar 370 FT-IR Thermo Nicolet and only noteworthy absorptions are listed. The ¹H-NMR (400 MHz) and the ¹³C-NMR (100 MHz) spectra were recorded on a Bruker Avance DRX-400 Fourier transformer spectrometer. Chemical shifts are reported in ppm downfield from TMS as internal standard. The mass spectra were scanned on a Varian Mat CH-7 at 70 eV. Elemental analyses were performed on a Thermo Finnigan Flash EA microanalyzer.

3-Acetyl-5-imino-1,4,6-triphenyl-4,5,6,8-tetrahydropyrimido [4,5-*c*]pyridazin-7(1H)-one (2). To a solution of (1) (10 mmol, 3.16 g) and phenyl isocyanate (10 mmol, 1.19 g) in dry dimethylformamide (5 mL), KOH (12 mmol 0.67 g) were added, and the mixture was stirred at room temperature for 5 h [monitored

by thin-layer chromatography (TLC) using chloroform:methanol 9:1]. Then, the reaction mixture was poured into water and neutralized with diluted HCl solution. The resulting solid was filtered, washed with water (2×20 mL), dried, and recrystallized from ethanol, respectively. Yellow powder, yield=70%; mp 286–288°C; ¹H-NMR (DMSO-*d*₆): δ 2.40 (s, 3H, CH₃-CO), 5.05 (br, 1H, NH), 5.25 (s, 1H, CH pyridazine), 7.10 (br s, 1H, C=NH), 7.20–7.7 (m, 15H, phenyl); ¹³C-NMR (DMSO-*d*₆): δ 25.8, 36.3, 86.1, 120.7, 124.6, 124.8, 125.1, 126.6, 128.8, 129.4, 131.4, 135.4, 137.3, 141.6, 146.2, 151.6, 154.0, 166.0, 192.1; MS (EI): *m/z* (%)=435 (M+), 391, 347; IR (KBr disk): ν 3383, 3183, 1679, 1621, 1599, 1521, 1379, 1188, 694 cm⁻¹; *Anal.* Calcd for C₂₆H₂₁N₅O₂: C, 71.71; H, 4.86; N, 16.08. Found: C, 71.69; H, 4.76; N, 16.06.

Ethyl N-(6-acetyl-4-cyano-2,5-diphenyl-2,5-dihydropyridazin-3-yl)formimidate (3). The solution of compound (1) (10 mmol, 3.16 g) and excess amount of triethylorthoformate (20 mL) in anhydride acetic acid (5 mL) were refluxed for about 6 h. After the completion of the reaction, which was monitored by TLC using chloroform:methanol (9:1), the solvent was evaporated under reduced pressure. The resulting precipitant was washed with water (2×20 mL), dried, and recrystallized from ethanol, respectively. Yellow powder, yield=90%; mp 137–135°C; ¹H-NMR (CDCl₃): δ 1.15 (t, 3H, CH₂CH₃), 2.45 (s, 3H, CH₃-CO), 4.15 (q, 2H, O-CH₂-), 5.05 (s, 1H, CH pyridazine), 7.20–7.60 (m, 10H, phenyl), 7.91 (s, 1H, N=CH-O); ¹³C-NMR (CDCl₃): 14.2, 25.8, 38.8, 61.7, 105.8, 116.3, 122.4, 122.5, 125.2, 126.9, 127.0, 127.6, 127.7, 130.5, 132.8, 132.9, 141.3, 142.2, 149.3, 152.0, 166.9, 191.6; MS (EI): *m/z* (%)=372 (M+); IR (KBr): ν 3068, 2982, 2202, 1686, 1637, 1198, 759, 702 cm⁻¹; *Anal.* Calcd for C₂₂H₂₀N₄O₂: C, 70.95; H, 5.41; N, 15.04. Found: C, 70.90; H, 5.39; N, 15.02.

N'-(6-Acetyl-4-cyano-2,5-diphenyl-2,5-dihydropyridazin-3-yl)formimidamide (4). To a solution of compound (3) (10 mmol, 3.72 g) in absolute ethanol (20 mL), 25% ammonium hydroxide solution (5 mL) was added. The solution was stirred at room temperature until the precipitate was formed. The resulting solid was washed with water (2×20 mL), dried, and recrystallized from ethanol, respectively. Yellow powder, yield = 93%; mp 240–242°C (decomp.); ¹H-NMR (CDCl₃): δ 2.39 (s, 3H, CH₃-CO), 4.32 (br s, 2H, NH₂), 5.00 (s, 1H, CH pyridazine), 7.20–7.60 (m, 10H, phenyl and 1H, N=CH-N); ¹³C-NMR (CDCl₃): 25.8, 38.8, 106.4, 116.3, 122.4, 122.5, 125.2, 126.7, 126.8, 127.5, 127.6, 130.5, 132.7, 132.8, 141.3, 143.1, 146.4, 149.3, 152.5, 191.6; MS (EI): *m/z* (%)=343 (M+); IR (KBr): ν 3412, 3330, 3191, 2198, 1671, 1651, 1595, 1563, 1423, 1221, 1140, 697 cm⁻¹; *Anal.* Calcd for C₂₀H₁₇N₅O: C, 69.96; H, 4.99; N, 20.40. Found: C, 69.94; H, 4.95; N, 20.39.

1-(5-Amino-1,4-diphenyl-1,4-dihydropyrimido[4,5-*c*]pyridazin-3-yl)ethanone (5). The mixture of compound (4) (10 mmol, 3.43 g) and sodium ethoxide (0.23 g sodium metal in 5 mL absolute ethanol) was refluxed for 5 h. The resulting precipitate was filtered, washed with ethanol (2×20 mL), and dried. Yellow powder, yield=35%; mp 295–297°C; ¹H-NMR (DMSO-*d*₆): δ 2.33 (s, 3H, CH₃-CO), 5.55 (s, 1H, CH pyridazine), 7.05 (br s, 2H, NH₂), 7.21–7.70 (m, 10H, phenyl), 8.05 (s, 1H, CH=N); ¹³C-NMR (CDCl₃): 24.5, 35.2, 97.2, 113.9, 114.0, 125.9, 127.9, 128.3, 128.4, 128.5, 128.6, 130.2, 130.3, 135.8, 145.4, 148.7, 152.7, 164.3, 166.8, 193.4; MS (EI): *m/z* (%)=343 (M+), 301, 266, 97, 77, 57; IR (KBr): ν 3402, 3329, 3178, 1671, 1655, 1564, 1487, 1423, 1222, 1141, 698 cm⁻¹;

Anal. Calcd for C₂₀H₁₇N₅O: C, 69.96; H, 4.99; N, 20.40. Found: C, 69.92; H, 4.95; N, 20.40.

5-Hydrazinyl-3-(1-hydrazonoethyl)-1,4-diphenyl-1,4-dihydropyrimido[4,5-*c*]pyridazine (7). A mixture of compound (3) (10 mmol, 3.72 g) and excess amount of hydrazine hydrate (60 mmol, 1.50 g) was refluxed in absolute ethanol (20 mL) for 5 h. After the completion of the reaction, which was monitored by TLC using chloroform:methanol (9:1), the reaction mixture was poured into an ice-water bath, and the resulting solid was filtered off, dried, and recrystallized from ethanol. Yellow powder, yield=85%; mp 266–269°C; ¹H-NMR (DMSO-*d*₆): δ 1.95 (s, 3H, CH₃), 5.65 (s, 1H, CH pyridazine), 5.75 (br s, 2H, NH₂), 6.60 (br s, 1H, NH), 6.90 (s, 2H, NH₂), 7.11–7.60 (m, 10H, phenyl), 7.85 (s, 1H, CH=N); ¹³C-NMR (DMSO-*d*₆): δ, 10.3, 36.2, 97.5, 114.7, 114.8, 125.9, 128.6, 128.8, 128.9, 129.1, 129.2, 129.3, 129.4, 136.3, 139.9, 141.9, 146.2, 153.9, 159.4, 166.1; MS (EI): *m/z* (%)=372 (M+), 356, 341, 281, 77, 57; IR (KBr): ν 3403, 3321, 3272, 1633, 1594, 745, 695 cm⁻¹; *Anal.* Calcd for C₂₀H₂₀N₈: C, 64.50; H, 5.41; N, 30.09. Found: C, 64.49; H, 5.38; N, 30.05.

Synthesis of 1-(1,4-diphenyl-5,7-dithioxo-1,4,5,6,7,8-hexahydropyrimido[4,5-*c*]pyridazin-3-yl)ethanone (8). A mixture of 6-acetyl-3-amino-2,5-diphenyl-2,5-dihydropyridazine-4-carbonitrile (1) (10 mmol, 3.16 g) and CS₂ (100 mmol, 7.6 g) in 10% ethanolic sodium hydroxide solution (20 mL) was heated under reflux for 7 h. After the completion of the reaction (monitored by TLC), the reaction mixture was cooled and added to crushed ice. The obtained precipitant was filtered, dried, and recrystallized from ethanol, respectively. Orange powder, yield=72%; mp >300°C; ¹H-NMR (acetone-*d*₆): δ 2.38 (s, 3H, CH₃-CO), 5.89 (s, 1H, CH pyridazine), 7.14 (br, 1H, NH), 7.21–7.70 (m, 10H, phenyl), 10.24 (br s, 1H, NH); ¹³C-NMR (acetone-*d*₆): δ 24.1, 36.5, 104.5, 125.8, 125.9, 126.7, 126.8, 128.0, 128.1, 128.2, 128.3, 128.5, 128.6, 141.9, 142.3, 145.6, 150.5, 176.6, 179.7, 196.2; MS (EI): *m/z* (%)=392 (M+), 318, 244, 135, 94, 76, 59, 43, 28; IR (KBr): ν 3125, 1683, 1533, 1478, 1375, 1269, 1141, 1122, 696 cm⁻¹; *Anal.* Calcd for C₂₀H₁₆N₄S₂O: C, 61.22; H, 4.11; N, 14.27; S, 16.34. Found: C, 61.20; H, 4.08; N, 14.24; S, 16.21.

General procedure for the synthesis of 1-(5,7-bis(alkylthio)-1,4-diphenyl-1,4-dihydropyrimido[4,5-*c*]pyridazin-3-yl)ethanone (9a-e). A mixture of 1-(1,4-diphenyl-5,7-dithioxo-1,4,5,6,7,8-hexahydropyrimido[4,5-*c*]pyridazin-3-yl)ethanone (8) (10 mmol, 3.92 g) and the appropriate alkyl halide (20 mmol) in 10% ethanolic sodium hydroxide solution (40 mL) was heated under reflux for 8 h. The reaction progress was monitored by TLC using chloroform:methanol (9:1). After the completion of the reaction, the mixture was cooled and poured into cold water. The obtained crude solid was filtered, dried, and recrystallized from ethanol, respectively.

1-(5,7-Bis(methylthio)-1,4-diphenyl-1,4-dihydropyrimido[4,5-*c*]pyridazin-3-yl)ethanone (9a). Yellow powder, yield=55%; mp 72–74°C; ¹H-NMR (CDCl₃): δ 2.36 (s, 3H, CH₃-CO), 2.44 (s, 3H, -SCH₃), 2.52 (s, 3H, -SCH₃), 5.47 (s, 1H, CH pyridazine), 7.22–7.67 (m, 10H, phenyl); ¹³C-NMR (CDCl₃): δ 12.8, 14.1, 25.0, 35.9, 105.8, 125.1, 125.2, 126.8, 127.6, 128.1, 128.2, 128.3, 128.4, 128.7, 128.8, 140.1, 141.3, 144.9, 151.4, 169.2, 169.3, 196.0; MS (EI): *m/z* (%)=420 (M+), 405, 375, 341, 200; IR (KBr): ν 2921, 1686, 1514, 1494, 1354, 1137, 1291, 694 cm⁻¹; *Anal.* Calcd for C₂₂H₂₀N₄S₂O: C, 62.83; H, 4.79; N, 13.32; S, 15.25. Found: C, 62.80; H, 4.77; N, 13.28; S, 15.21.

1-(5,7-Bis(ethylthio)-1,4-diphenyl-1,4-dihydropyrimido[4,5-*c*]pyridazin-3-yl)ethanone (9b). Yellow powder, yield=53%; mp 55–58°C; ¹H-NMR (CDCl₃): δ 1.24 (t, 3H, -SCH₂CH₃),

1.34 (t, 3H, $-\text{SCH}_2\text{CH}_3$), 2.44 (s, 3H, CH_3CO), 2.91 (q, 2H, $-\text{SCH}_2-$), 3.20 (d of q, 2H, $-\text{SCH}_2-$), 5.48 (s, 1H, CH pyridazine), 7.24–7.65 (m, 10H, phenyl); ^{13}C -NMR (CDCl_3): δ 14.4, 14.7, 24.4, 24.9, 25.3, 36.0, 105.9, 125.2, 125.3, 126.9, 127.6, 128.4, 128.5, 128.6, 128.7, 128.8, 128.9, 140.1, 141.3, 145.0, 151.8, 168.8, 169.2, 196.0; MS (EI): m/z (%) = 448 (M+), 419, 368; IR (KBr): ν 2921, 1690, 1514, 1493, 1355, 1133, 694 cm^{-1} ; Anal. Calcd for $\text{C}_{24}\text{H}_{24}\text{N}_4\text{S}_2\text{O}$: C, 64.26; H, 5.39; N, 12.49; S, 14.30. Found: C, 64.20; H, 5.31; N, 12.42; S, 14.20.

1-(5,7-Bis(propylthio)-1,4-diphenyl-1,4-dihydropyrimido[4,5-c]pyridazin-3-yl)ethanone (9c). Yellow powder, yield = 48%; mp 50–53°C; ^1H -NMR (CDCl_3): δ 0.99 (t, 3H, $-\text{SCH}_2\text{CH}_2\text{CH}_3$), 1.01 (t, 3H, $-\text{SCH}_2\text{CH}_2\text{CH}_3$), 1.59 (m, 2H, $-\text{SCH}_2\text{CH}_2\text{CH}_3$), 1.65 (m, 2H, $-\text{SCH}_2\text{CH}_2\text{CH}_3$), 2.43 (s, 3H, CH_3CO), 2.85 (t, 2H, $-\text{SCH}_2-$), 3.23 (d of t, 2H, $-\text{SCH}_2-$), 5.48 (s, 1H, CH pyridazine), 7.21–7.63 (m, 10H, phenyl); ^{13}C -NMR (CDCl_3): δ 13.4, 13.5, 22.6, 23.0, 24.9, 31.8, 32.8, 35.9, 105.9, 125.2, 125.3, 126.8, 127.6, 128.1, 128.2, 128.3, 128.4, 128.7, 128.8, 140.1, 141.4, 145.0, 151.8, 168.9, 169.2, 196.0; MS (EI): m/z (%) = 476 (M+), 433, 397; IR (KBr): ν 2958, 2925, 1686, 1511, 1493, 1351, 1135, 693 cm^{-1} ; Anal. Calcd for $\text{C}_{26}\text{H}_{28}\text{N}_4\text{S}_2\text{O}$: C, 65.51; H, 5.92; N, 11.75; S, 13.45. Found: C, 65.46; H, 5.87; N, 11.65; S, 13.40.

1-(5,7-Bis(butylthio)-1,4-diphenyl-1,4-dihydropyrimido[4,5-c]pyridazin-3-yl)ethanone (9d). Yellow powder, yield = 50%; mp 68–70°C; ^1H -NMR (CDCl_3): δ 0.86 (t, 3H, $-\text{SCH}_2\text{CH}_2\text{CH}_2\text{CH}_3$), 0.92 (t, 3H, $-\text{SCH}_2\text{CH}_2\text{CH}_2\text{CH}_3$), 1.29 (m, 2H, $-\text{SCH}_2\text{CH}_2\text{CH}_2\text{CH}_3$), 1.44 (m, 2H, $-\text{SCH}_2\text{CH}_2\text{CH}_2\text{CH}_3$), 1.52 (m, 2H, $-\text{SCH}_2\text{CH}_2\text{CH}_2\text{CH}_3$), 1.62 (m, 2H, $-\text{SCH}_2\text{CH}_2\text{CH}_2\text{CH}_3$), 2.44 (s, 3H, CH_3CO), 2.84–2.92 (m, 2H, $-\text{SCH}_2-$), 3.20 (d, 2H, $J = 6.5 \text{ Hz}$, $-\text{SCH}_2-$), 5.48 (s, 1H, CH pyridazine), 7.23–7.63 (m, 10H, phenyl); ^{13}C -NMR (CDCl_3): δ 13.7, 13.8, 22.0, 22.1, 24.9, 29.6, 30.6, 31.2, 31.7, 35.9, 105.9, 125.2, 125.3, 126.8, 127.6, 128.1, 128.2, 128.3, 128.4, 128.7, 128.8, 140.1, 141.4, 144.9, 151.8, 168.9, 169.3, 196.0; MS (EI): m/z (%) = 504 (M+), 447, 425, 328; IR (KBr): ν 2958, 2929, 2871, 1686, 1511, 1493, 1351, 1136, 761, 694 cm^{-1} ; Anal. Calcd for $\text{C}_{28}\text{H}_{32}\text{N}_4\text{S}_2\text{O}$: C, 66.63; H, 6.39; N, 11.10; S, 12.71. Found: C, 66.59; H, 6.31; N, 11.08; S, 12.64.

1-(5,7-Bis(benzylthio)-1,4-diphenyl-1,4-dihydropyrimido[4,5-c]pyridazin-3-yl)ethanone(9e). Yellow powder, yield = 34%; mp 70–72°C; ^1H -NMR (CDCl_3): δ 2.42 (s, 3H, CH_3-CO), 5.44 (s, 1H, CH pyridazine), 4.12 (d, 2H, $-\text{SCH}_2-$), 4.40 (d, 2H, $-\text{SCH}_2-$), 7.02–7.66 (m, 20H, phenyl); ^{13}C -NMR (CDCl_3): δ 24.9, 34.1, 35.0, 35.9, 106.0, 125.4, 125.5, 127.0, 127.1, 127.3, 127.7, 128.2, 128.3, 128.4, 128.5, 128.6, 128.7, 128.8, 128.9, 128.8, 128.9, 129.0, 129.1, 129.2, 129.3, 136.9, 137.7, 139.9, 141.4, 145.0, 151.9, 168.3, 168.7, 195.8; MS (EI): m/z (%) = 572 (M+), 541, 482, 403; IR (KBr): ν 3023, 1683, 1511, 1492, 1351, 1131, 693 cm^{-1} ; Anal. Calcd for $\text{C}_{34}\text{H}_{28}\text{N}_4\text{S}_2\text{O}$: C, 71.30; H, 4.93; N, 9.78; S, 11.20. Found: C, 71.27; H, 4.91; N, 9.77; S, 11.17.

Theoretical calculations. In this study, the calculations for molecular equilibrium geometry and vibrational spectra of all molecules were performed by means of the Gaussian 03 W software package [24]. The mPW1PW91 method and 6-31G(d) basis set were utilized for optimization and NMR calculations [25]. This level of density functional theory has been mentioned as a powerful one in producing NMR spectra [26,27]. Gauge-independent atomic orbital (GIAO) method [28–31] was applied to provide NMR spectra. The chemical shift of TMS as the reference was calculated by the same level. The chemical shifts were obtained by the GaussView 4.1 [32], the graphical

interface for Gaussian programs, which gives a visual representation of the calculated data. The polarizable continuum model [33] was chosen for the self-consistent reaction-field calculations for different solutions. The polarizable continuum model was applied within the mPW1PW91/6-31G(d) level to predict the solvent effects on the structure.

Structure optimization. Three dimensional structures of compounds (2), (5), (7), and (9a–e) were simulated in HyperChem 7.5 using MM⁺ method (RMS gradient = 0.1 kcal mol⁻¹) (HyperChem® Release 7, Hypercube Inc., <http://www.hyper.com>). In the second optimization, output files were minimized under Semi empirical AM1 methods (Convergence limit = 0.01; Iteration limit = 50; RMS gradient = 0.1 kcal mol⁻¹; Polak-Ribiere optimizer algorithm). Crystal structures of AKT1 inhibitor VIII were retrieved from RCSB Protein Data Bank (PDB entry: 3O96).

Acknowledgments. The authors gratefully acknowledge Ferdowsi University of Mashhad for partial support of this project (3/19530).

REFERENCES AND NOTES

- [1] Kettle, J. G.; Brown, S.; Crafter, C.; Davies, B. R.; Dudley, P.; Fairley, G.; Faulder, P.; Fillery, S.; Greenwood, H.; Hawkins, J.; James, M.; Johnson, K.; Lane, C. D.; Pass, M.; Pink, J. H.; Plant, H.; Cosulich, S. C. *J Med Chem* 2012, 55, 1261.
- [2] Altomare, C.; Cellamare, S.; Summo, L.; Catto, M.; Carotti, A. *J Med Chem* 1998, 41, 3812.
- [3] Giovannoni P. M.; Vergelli, C.; Biancalani, C.; Cesari, N.; Graziano, A.; Biagini, P.; Gracia, J.; Gavaldà, A.; Piaz, V. D. *J Med Chem* 2006, 49, 5363.
- [4] Rimaz, M.; Khalafy, J.; Pesyan, N. N.; Prager, R. H. *Aust J Chem* 2010, 63, 507.
- [5] Giovannoni, M. P.; Vergelli, C.; Cilibrizzi, A.; Crocettia, L.; Biancalani, C.; Graziano, A.; Piaz, V. D.; Loza, I. M.; Cadavid, M. I.; Diaz, J. L.; Gavaldà, A. *Bioorg Med Chem* 2010, 18, 7890.
- [6] Duffy, J. P.; Harrington, E. M.; Salituro, F. G.; Cochran, J. E.; Green, J.; Gao, H.; Bemis, G. W.; Evindar, G.; Galullo, V. P.; Ford, P. J.; Germann, U. A.; Wilson, K. P.; Bellon, S. F.; Chen, G.; Taslimi, P.; Jones, P.; Huang, C.; Pazhanisamy, S.; Wang, Y. M.; Murcko, M. A.; Su, M. S. *S. ACS Med Chem Lett* 2011, 2, 758.
- [7] Pollak, A.; Stanovnik, B.; Tisler, M. *J Org Chem* 1971, 36, 2457.
- [8] Mallory, W. R.; Morrison, R. W. *J J Org Chem* 1980, 45, 3919.
- [9] Mallory, W. R.; Morrison, R. W. J.; Styles, V. L. *J Org Chem* 1982, 47, 667.
- [10] Styles, V. L.; Morrison, Jr. R. W. *J Org Chem* 1982, 47, 585.
- [11] Morrison, R. W. J.; Styles, V. L. *J Org Chem* 1982, 47, 674.
- [12] Turbiak, A. J.; Kampf, J. W.; Showalter, H. D. H. *Tetrahedron Lett* 2010, 51, 1326.
- [13] Khalafy, J.; Rimaz, M.; Panahi, L.; Rabiei, H. *Bull Korean Chem Soc* 2011, 32, 2428.
- [14] Eftekhari-Sis, B.; Zirak, M.; Akbari, A. *Chem Rev* 2013, 113, 2958.
- [15] Wu, W.; Voegtli, W. C.; Sturgis, H. L.; Dizon, F. P.; Vigers, G. P. A.; Brandhuber, B. *J PLOS ONE* 2010, 5, e12913.
- [16] Al-Awadi, N. A.; Ibrahim, M. R.; Al-Etaibi A. M.; Elnagdi, M. H. *ARKIVOC* 2011, ii, 310.
- [17] Al-Mousawi, S. M.; Mustafa, M. S.; Elnagdi, M. H. *Tetrahedron Lett* 2009, 50, 6411.
- [18] Sheibani, H.; Amrollahi, M. A.; Esfandiarpour, Z. *Mol Divers* 2010, 14, 277.
- [19] Rashad, A. E.; Hegab, M. I.; Abdel-Megeid, R. E.; Fathalla, N.; Abdel-Megeid, F. M. E. *Eur J Med Chem* 2009, 44, 3285.
- [20] Al-Afaleq, E. I.; Abubshait, S. A. *Molecules* 2001, 6, 621.
- [21] Hassan, N. A. *Molecules* 2000, 5, 826.

- [22] Lodewyk, M. W.; Siebert, M. R.; Tantillo, D. *J Chem Rev* 2012, 112, 1839.
- [23] Katritzky, A. R. *Adv Heterocycl Chem Academic Press* 2010, 101, 162.
- [24] Frisch, M. J.; Trucks, G. W.; Schlegel, H. B.; Scuseria, G. E.; Robb, M. A.; Cheeseman, J. R.; Montgomery, J. A., Jr.; Vreven, T.; Kudin, K. N.; Burant, J. C.; Millam, J. M.; Iyengar, S. S.; Tomasi, J.; Barone, V.; Mennucci, B.; Cossi, M.; Scalmani, G.; Rega, N.; Petersson, G. A.; Nakatsuji, H.; Hada, M.; Ehara, M.; Toyota, K.; Fukuda, R.; Hasegawa, J.; Ishida, M.; Nakajima, T.; Honda, Y.; Kitao, O.; Nakai, H.; Klene, M.; Li, X.; Knox, J. E.; Hratchian, H. P.; Cross, J. B.; Adamo, C.; Jaramillo, J.; Gomperts, R.; Stratmann, R. E.; Yazyev, O.; Austin, A. J.; Cammi, R.; Pomelli, C.; Ochterski, J. W.; Ayala, P. Y.; Morokuma, K.; Voth, G. A.; Salvador, P.; Dannenberg, J. J.; Zakrzewski, V. G.; Dapprich, S.; Daniels, A. D.; Strain, M. C.; Farkas, O.; Malick, D. K.; Rabuck, A. D.; Raghavachari, K.; Foresman, J. B.; Ortiz, J. V.; Cui, Q.; Baboul, A. G.; Clifford, S.; Cioslowski, J.; Stefanov, B. B.; Liu, G.; Liashenko, A.; Piskorz, P.; Komaromi, I.; Martin, R. L.; Fox, D. J.; Keith, T.; Al-Laham, M. A.; Peng, C. Y.; Nanayakkara, A.; Challacombe, M.; Gill, P. M. W.; Johnson, B.; Chen, W.; Wong, M. W.; Gonzalez, C.; Pople, J. A. *Gaussian 03, revision C.02*; Gaussian, Inc.: Wallingford, CT, 2004.
- [25] Adamo, C.; Barone, V. *J Chem Phys* 1998, 108, 664.
- [26] Bakavoli, M.; Eshghi, H.; Shiri, A.; Afrough, T.; Tajabadi, J. *J Tetrahedron* 2013, 69, 8470.
- [27] Sarotti, A. M.; Pellegrinet, S. C. *J Org Chem* 2009, 74, 7254.
- [28] Ditchfield, R. *J Chem Phys* 1972, 56, 5688.
- [29] Ditchfield, R. *Mol Phys* 1974, 27, 789.
- [30] Rohlfing, C. M.; Allen, L. C.; Ditchfield, R. *J Chem Phys* 1984, 87, 9.
- [31] Wolinski, K.; Hinton, J. F.; Pulay, P. *J Am Chem Soc* 1990, 112, 8251.
- [32] Dennington, R.; Keith, T.; Millam, J. *GaussView, Version 4.1*, Semichem Inc., Shawnee Mission, KS, 2007, 1, 93.
- [33] Tomasi, J.; Persico, M. *Chem Rev* 1994, 94, 2027.